Estuarine, Coastal and Shelf Science 92 (2011) 437–445

Contents lists available at ScienceDirect

Estuarine, Coastal and Shelf Science

journal homepage: www.elsevier.com/locate/ecss

Suitability of spaceborne multispectral data for inter-tidal sediment characterization: A case study

Elsy Ibrahim*, Jaak Monbaliu

Hydraulics Laboratory, Department of civil engineering, Katholieke Universiteit Leuven, Kasteelpark Arenberg 40, 3001 Heverlee, Belgium

ARTICLE INFO

Article history:
Received 9 November 2010
Accepted 28 January 2011
Available online 16 February 2011

Keywords:
remote sensing
hyperspectral
multispectral
unsupervised classification
mixture of Gaussians
inter-tidal sediments
Molenplaat

ABSTRACT

The aim of this study is to assess the suitability of four spaceborne multispectral sensors (Spot 5 HRG, Landsat 5 TM, Landsat 7 ETM+, and IKONOS) for inter-tidal sediment characterization, in comparison to a hyperspectral image of 4 m × 4 m spatial resolution and 116 spectral bands. Four sediment properties were considered: organic matter content, moisture content, chlorophyll *a* content, and mud content. The utilized data were a hyperspectral image and its accompanying field data. The methodology included spectral and spatial resampling of this image to the properties of the spaceborne multispectral sensors. Then, these resampled data were analyzed by means of unsupervised classification. The results showed that spaceborne multispectral data have the potential for sediment characterization. Yet, compared to the hyperspectral image, the characterization of the different properties generally decreased. The results showed the spectral suitability of Landsat sensors to characterize all properties and the spectral and spatial suitability of all sensors to characterize chlorophyll *a* content.

1. Introduction

The important geochemical processes that occur on inter-tidal flats define sediment stability in relation to the physical, biological, and chemical properties of sediments (Silva et al., 2005). The erodibility of sediments depends on their physical structure as non-cohesive sediments are less stable than cohesive ones (Mitchener and Torfs, 1996). Furthermore, the presence of microphytobenthic algae and macrofaunal species can either stabilize or destabilize sediments (Austen et al., 1999). To investigate these processes, good field knowledge is required. Since accurate data collection on inter-tidal flats is often costly, inefficient, or even unattainable, remote sensing can be a fine and resourceful alternative.

The remote sensing concept can be used for this purpose due to the interaction of light with matter, resulting in a reflected signal that provides information on the surface properties. For example, fine particles or mud particles (grain size < 0.63 μm) result in absorption at specific clay absorption features (Hunt, 1977). Furthermore, an increase in moisture content leads to an overall decrease of the reflectance spectrum (Muller and Decamps, 2000; Weidong et al., 2002). Yet, at a soil dependent value of moisture content referred to as "the cut-off thickness", reflectance increases as moisture content increases (Neema et al., 1987). Regarding the biological properties of sediments, an increase in the chlorophyll *a* (chl *a*) pigment, an indicator of the presence of micro-phytobenthos, on the sediment surface leads to an emphasis of the absorption dip at around 673 nm of the spectrum (Carrère et al., 2004; Murphy et al., 2005).

Remote sensing techniques are in rapid evolution whereby numerous and diverse research possibilities continuously arise, especially with the increasing number of hyperspectral and multi-spectral sensors. Nowadays, choices have to be made regarding the suitable platforms and spectral, spatial, and temporal resolutions that are to be used for a certain objective. Various remote sensing acquisitions and applications have led to a successful characterization of inter-tidal sediments (Brockmann and Stelzer, 2008). For many, airborne hyperspectral sensors are essential instruments for such studies as they acquire images in tens of spectral bands providing a huge amount of useful data for sediment characterization (Yates et al., 1993; Bryant et al., 1996; Thomson et al., 1998; Rainey et al., 2003; Smith et al., 2004; Deronde et al., 2006). Furthermore, such sensors offer various possibilities due to their programmable nature that allows diverse temporal, spectral, and spatial resolutions. Scheduling the acquisition of airborne imagery is essential to study inter-tidal sediments as it is mostly carried out at low tide. Although hyperspectral data are powerful and valuable, a flight campaign is relatively expensive leading to only a few occasional acquisitions (Thomson et al., 2003; Dalponte et al., 2009).

* Corresponding author.
E-mail address: elsy.ibrahim@gmail.com (E. Ibrahim).

0272-7714/$ – see front matter © 2011 Elsevier Ltd. All rights reserved.
doi:10.1016/j.ecss.2011.01.017

Furthermore, due to its high dimensionality, image processing is complex: the "curse of dimensionality" (Hughes, 1968).

The use of spaceborne multispectral imagery widens the possibilities of remote sensing applications in studying and monitoring inter-tidal flats. Many state-of-art multispectral spaceborne sensors have been utilized for environmental applications on inter-tidal flats (Ryu et al., 2004; Dong et al., 2005; Belluco et al., 2006; Sorensen et al., 2006; Barillé et al., 2010). Specifically, studies have tested or utilized spaceborne multispectral data to carry out morphologic change estimation (Ryu et al., 2008). Such data have been also used to characterize sediment properties, with emphasis on grain size distribution (Yates et al., 1993; Choi et al., 2010; Huang et al., 2010), showing the usefulness of sensors such as IKONOS and Landsat 5 TM, using diverse approaches.

Spaceborne multispectral sensors provide data in a wide range of spatial and spectral scales, and their cost is relatively low. They allow the utilization of imagery from different sensors, and thus, increasing the possibility of obtaining a larger number of useful images to study temporal evolution. Yet, such sensors have their shortcomings especially due to their lower operational flexibility.

The objective of this paper is to investigate the applicability, regarding sediment characterization, of four commonly used spaceborne multispectral sensors, in comparison to a hyperspectral sensor. The sensors are Spot 5 HRG, Landsat 5 TM, Landsat 7 ETM+, and IKONOS. They were chosen for their popular usage in environmental applications and their high to moderate spatial resolution. The spectral and spatial aspects of these sensors were investigated in this paper in an independent manner.

2. Study area and data set

2.1. Study area

The Molenplaat is an inter-tidal flat that has been a nature reserve since 1997. It is about 61 ha and located in the Western-Schelde estuary in the Netherlands (Fig. 1). The Schelde estuary is internationally recognized for its important role in nature conservation. It has one of the largest wading bird populations in Western Europe and several rare habitat types such as freshwater tidal marshes. Yet, this estuary is an important shipping route and holds sites of heavy industry (Herman et al., 2001; Adam, 2009).

2.2. Airborne hyperspectral data

On the 8th of June 2004, an image was acquired of the Molenplaat by means of the Hyperspectral Mapper (HyMap™) sensor at low tide and in cloud-free conditions (4 m × 4 m pixel size). Table 1 gives a summary of the useful 116 bands of the HyMap™ image. For each of the modules – visible (VIS), near-infrared (NIR), and short wave-infrared (SWIR) – the number of bands, the spectral range, and the full width at half maximum (fwhm) are listed. Deronde et al. (2006) gives a detailed overview of the flight campaign and image acquisition, and Ibrahim and Monbaliu (2009) gives details regarding all the spectral bands and settings of the image.

2.3. Field data

Field sampling at 24 sites of the Molenplaat was carried out at low tide, on the day of the overflight. The coordinates of these sites were determined by means of a differential geographical positioning system (DGPS). To account for the variability within one pixel, two or three replicates were sampled at each site.

Surface sediment was scraped, collected, and analyzed for moisture content (MC), organic matter content (OM), and grain size distribution. For chlorophyll *a* determination, the upper 2 mm of sediment was frozen using a contact corer, which freezes all photosynthetically active cells as well as the bulk of sediment chlorophyll (Ford and Honeywill, 2002). The analysis of all these samples was carried out by the methods described by Deronde et al. (2006).

3. Methodology

3.1. The hyperspectral cube

A hyperspectral image is generally a "cube" of data, whereby two axes refer to location, and a third axis refers to spectral dimensionality. In this paper, spatial location was not taken into account, whereby a pixel was only described by its reflectance value per spectral band, without including the effect of neighboring pixels. Therefore, an image can be seen as a set of N pixels. Each pixel is represented by an n-dimensional vector $\mathbf{x}_k$, referred to as a feature vector, where $k \in [1, N]$, and n is the number of features (bands). This feature vector contains the values of a pixel's reflectance spectrum. The combination of these N feature vectors is the $N \times n$ image $\mathbf{X}$.

3.2. The spectral aspect

Spectral resampling is a form of convolution that allows to form an image as seen by a particular sensor from an image with higher spectral resolution. A sensor follows a certain spectral response

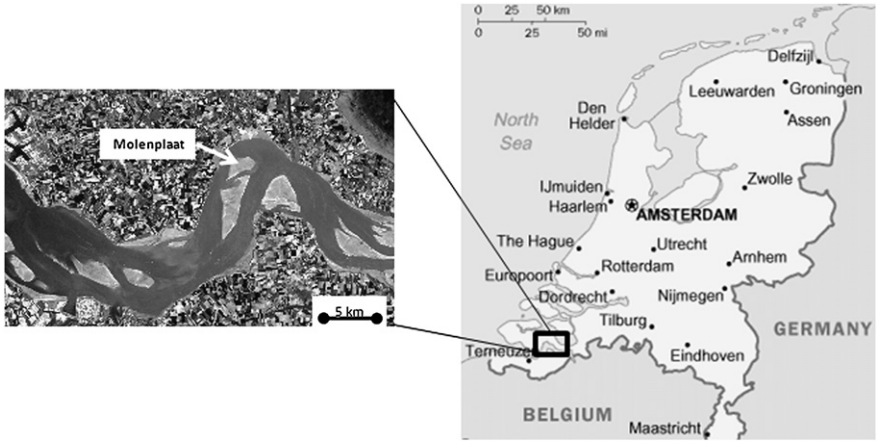

Fig. 1. The location of the Molenplaat and its surroundings.

Table 1
Characteristics of HyMap™ image acquired on the 8th of June 2004, excluding noisy bands.

Module	Spectral range [nm]	Band width [nm]	Fwhm [nm]	Number of bands [-]
VIS	450–890	15–16	15	30
NIR	890–1350	15–16	15	32
SWIR1	1400–1800	15–16	13	32
SWIR2	1950–2480	18–20	17	32

function that is characterized by the central wavelengths and the fwhm of each spectral band. This function is used to alter the spectral resolution of a certain data set to that of the considered sensor. When this function is not known for a sensor, an assumption of normality of spectral response is considered, and an approximation using Gaussian functions can be done (Schläpfer et al., 1999).

The hyperspectral image considered in this study and its accompanying field data have been proven to be suitable for sediment characterization of the Molenplaat (Adam et al., 2006; Deronde et al., 2006). A spectral resampling of this HyMap™ image was carried out to the spectral resolution of the considered multispectral sensors (Table 2). The spectral response functions of each of these sensors were known (ENVI, 2009). The response function of HyMap™ was not available and therefore approximated using Gaussian functions, knowing the mean and the full width at half maximum of each band.

3.3. The spatial aspect

Besides the spectral resolution of a sensor, the spatial resolution is a fundamental aspect that affects the ability to characterize specific entities in an image. It is defined by the combination of the height and the instantaneous field of view of the acquiring sensor (Atkinson and Curran, 1995; Lillesand and Kiefer, 2000). The spatial resolution issue is investigated since each resolution of a different type of imagery offers a distinctive perception and reveals different processes (Sadowski and Sarno, 1976).

The traditional selection of a spatial resolution for a certain application has been mostly based on experience, intuition, and data availability. In general, researchers have the tendency to choose imagery with the highest available or affordable resolution.

Table 2
Spectral and spatial properties of the four spaceborne multispectral sensors.

Sensor	Number of bands [-]	Band range [μm]	Pixel size [m]
IKONOS	4	0.445–0.516	4
		0.506–0.595	4
		0.632–0.698	4
		0.757–0.853	4
Landsat 5 TM	6	0.45–0.52	30
		0.52–0.60	30
		0.63–0.69	30
		0.76–0.90	30
		1.55–1.74	30
		2.08–2.35	30
Landsat 7 ETM+	6	0.45–0.515	30
		0.525–0.605	30
		0.63–0.69	30
		0.75–0.90	30
		1.55–1.75	30
		2.09–2.35	30
Spot 5 HRG	4	0.50–0.59	10
		0.61–0.68	10
		0.78–0.89	10
		1.58–1.75	20

This resolution can be too low, leading to a loss of required information, or too high, leading to "too much" information, and therefore, resulting in high cost, limited number of images, and low efficiency in data interpretation.

Several researchers began to address this issue more objectively, whereby they investigated measures or criteria for the selection of appropriate spatial resolutions. According to Woodcock and Strahler (1987), this selection depends on three main factors: the kind of information required, the methods used to extract the information from the imagery, and the spatial structure of the scene itself. Several approaches can be used to study spatial patterns in imagery (Atkinson and Tate, 2000; Curran, 2001; Rahman et al., 2003; Foody et al., 2004; Crawley, 2007).

Since the aim of this paper is limited to testing the applicability of the four multispectral sensors, a simple approach was used whereby the original HyMap™ was spatially resampled to the resolution of these sensors. The spatial resampling procedure was based on the "pixel aggregation" concept whereby the pixels that fall within the coverage of the new resampled pixel were averaged. A weight was used for each pixel based on its contribution to the new pixel. The loss of information by using such lower spatial resolution was assessed using unsupervised classification and field data.

3.4. Unsupervised classification

3.4.1. About unsupervised classification

Classification of imagery is a basic and centrally utilized image processing tool for sediment characterization. Unsupervised classification groups the data into clusters while maximizing inter-class variability and minimizing intra-class variability, without referring to field knowledge (Lillesand and Kiefer, 2000). Yet, field knowledge is important to understand what the identified clusters represent. A successful unsupervised classification implies that the data are clustered in a meaningful manner. When used for sediment characterization, the resulting clusters represent the main spectrally distinguishable groups in the data. Since the spectra vary with sediment properties, these groups can represent important sediment types.

Unsupervised classification has been successfully used to characterize certain inter-tidal sediment properties (Doerffer and Murphy, 1989; Smith et al., 2004; Adam et al., 2006), even though this type of classification is generally less popular than supervised classification. However, unsupervised classification is essential for inaccessible areas found on inter-tidal flats. It assists in the planning of field campaigns and explains certain results of supervised classification (Ibrahim et al., 2009).

The basic aim of a classification is for an unclassified feature vector $\mathbf{x}_k$, belonging to a data set $\mathbf{X}$, to be affiliated to one of several specified groups. The first step is to find the probability of an unclassified feature vector to belong to each group. These probabilities are conditional and are referred to as a posteriori probabilities (Theodoridis and Koutroumbas, 1999). Depending on the classification approach, a classifier computes either the maximum of these probabilities or the maximum of a defined function of them. An unclassified feature vector is then assigned to belong to the group corresponding to this maximum.

3.4.2. Unsupervised classification using mixture of Gaussians approach

In this paper, the unsupervised scheme used was the mixture of Gaussians approach and was performed by means of the Mixture Modeling software (MIXMOD) by Biernacki et al. (2006). It is a model-based approach, i.e. it is constituted of models suitable for describing each cluster. It is a powerful approach for sediment characterization (Ibrahim et al., 2009). It optimizes the fit between

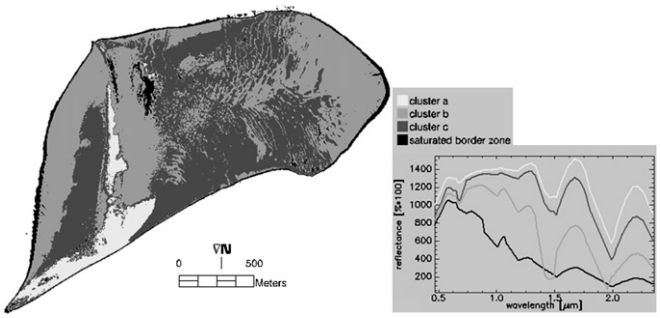

Fig. 2. The four final clusters of the MG classification of the hyperspectral image and their mean reflectance spectra.

a cluster of data and a specified model, whereby clusters are considered as various Gaussian distributions centered according to their covariance structure (Bozdogan, 1993; Bozdogan, 1994a; Beaven et al., 2000). Therefore, spectra $\mathbf{x}_k$, of n dimensions, belonging to $\mathbf{X}$, were assumed to arise from a probability distribution of the following density (Biernacki et al., 2006):

$$f(\mathbf{x}_k;\theta) = \sum_{i=1}^{I} P_i \varphi(\mathbf{x}_k; v_i, \mathbf{cov}_i) \quad (1)$$

P_i are the mixing proportions where $P_i \geq 0$, and $\sum_{i=1}^{I} P_i = 1$. Each proportion denotes the prior probability that a data point is generated by a mixture component i. v_i and $\mathbf{cov}_i$ denote the mean and the covariance matrix of the distribution. The vector parameters to be estimated are denoted by θ, i.e. $\theta = (P_i, \ldots, P_I, v_i, \ldots, v_I, \mathbf{cov}_i, \ldots, \mathbf{cov}_I)$.

$\varphi(\mathbf{x}_k; v_i, \mathbf{cov}_i)$ is of an n-dimensional density Gaussian distribution representing density component i:

$$\varphi(\mathbf{x}_k; v_i, \mathbf{cov}_i) = \frac{1}{\sqrt{(2\pi)^n |\mathbf{cov}_i|}} \exp\left(-\frac{1}{2}\left(\mathbf{x}_k - v_i^T \mathbf{cov}_i^{-1}\right)(\mathbf{x}_k - v_i)\right) \quad (2)$$

To find the mixture components, the expectation-maximization algorithm (EM) can be utilized (Dempster et al., 1977), where it assigns the a posteriori probabilities to each component density of the mixed Gaussian model with respect to each spectrum. Clusters are assigned by selecting the component that maximizes the a posteriori probabilities.

This Gaussian density model leads to (hyper) ellipsoidal classes, whose geometric characteristics are based on the eigenvalue decomposition of the covariance matrix. To be limited to this type of ellipsoidal property of the classes leads to fitting the data in clusters of equivalent features i.e. the shape, size, and orientation of the classes. Depending on the parameterization of the covariance matrix, models allow the fixing of cluster properties in various combinations, resulting in different model types (Banfield and Raftery, 1993; Biernacki et al., 2006). Bayesian Information Criterion (BIC) is used to choose the most descriptive of those models. It is a commonly used criterion to compare models with different parameterization and/or components since it effectively describes the data without the use of too many parameters (Fraley and Raftery, 1998). Therefore, the model with the smallest BIC value was chosen as the most suitable. The calculation was stopped using a threshold of 10^{-4} for the relative change of the likelihood criterion.

The algorithm was initiated with the selection of random seed pixels. Yet, due to its heuristic nature, it does not always attain global optimum solutions, but rather local optima. As a result, the classification was carried out several times (between 10 and 100, depending on the size of the data). The classification with the most suitable initiation was chosen based on the best classification represented by the lowest BIC values.

When carrying out unsupervised classification of the HyMap™ image of the Molenplaat, its high dimensionality caused calculation and efficiency drawbacks. Based on the work by Ibrahim et al. (2009) and the high correlation between the contiguous bands of the hyperspectral image, one out of five consecutive features were selected, leading to 24 spectrally representative bands of the considered parts of the electromagnetic spectrum.

3.4.3. Number of clusters

One of the basic steps of cluster analysis is to specify the number of clusters that the data is to be grouped into. The number of

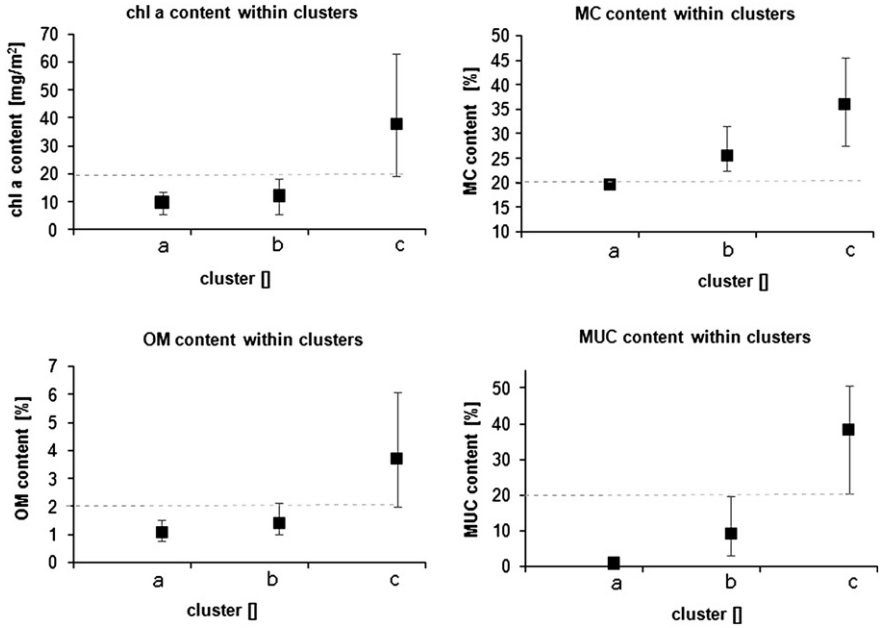

Fig. 3. The distribution of the field data within the resulting clusters of the original hyperspectral image - the mean, and 10th and 90th interquartile range of the field data are shown.

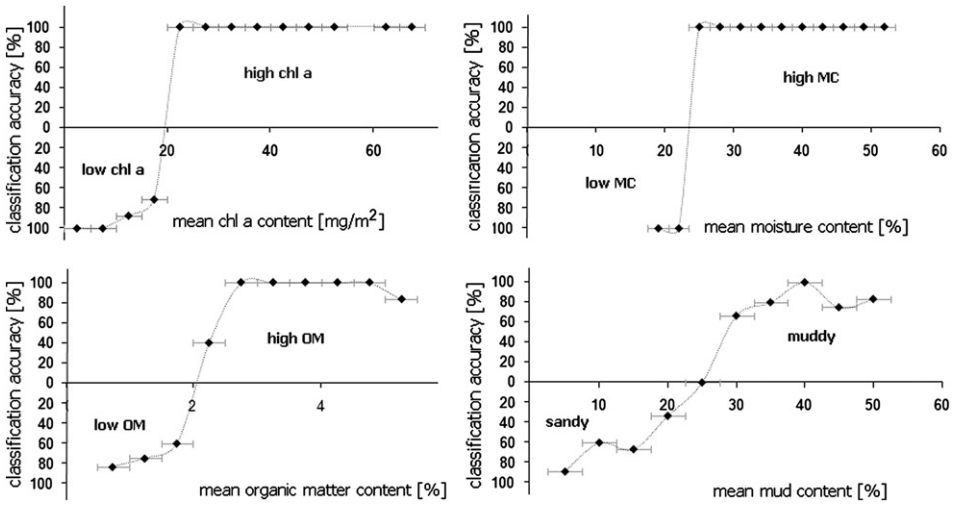

Fig. 4. The classification accuracy of field data with respect to ranges (5 mg/m^2 for chl *a* content, 3% for MC, 0.5% for OM, and 5% of MUC) of a property's content as derived from the original hyperspectral image.

clusters can be considered to vary between 1 and the smallest integer larger than $N^{0.3}$, where N is the number of pixels in an image (Bozdogan, 1994b; Biernacki et al., 2006; Kostov and McErlean, 2006). This is a rule of thumb that tries to ensure that the number of required parameters of the mixture models do not exceed the number of pixels. The normalized entropy criterion (NEC) (Biernacki et al., 2006) can be used to choose the most suitable number of sediment type clusters in an image (Ibrahim et al., 2009). NEC measures how well-separated the resulting clusters are with respect to different number of clusters, where the minimum values of NEC would indicate an appropriate division (Celeux and Soromenho, 1996).

Although NEC is a powerful criterion for finding the number of clusters in a data set, it could happen to be too parsimonious. Therefore, the number of clusters recommended by NEC was treated further. Each cluster was then divided individually by means of MG into a new specific number of clusters based on NEC. This resulted in a divisive, top-down hierarchical approach. Therefore, after the first clusters were identified, they were split recursively as one moves down the hierarchy. The two-step procedure was repeated until a decision was made to stop the splitting.

3.4.4. Clustering assessment

The Jeffries-Matusita (JM) separability measure and the percentage of correct clustering of field data were used. JM mainly calculates a mean distance for each cluster to all other clusters by averaging the distance between a specific cluster and the rest of the clusters (Klein et al., 2005). This is computed in a pairwise manner, values range from 0 to 2.0, and indicate how well the clusters are statistically separate. Values greater than 1.80 indicate that a cluster pair has a good separability.

After clustering the original hyperspectral image, the geographical location of each sampling site was affiliated to a resulting cluster. When a sampling site was located at the border between two or more clusters, it was excluded from the data set as it would not be representative of any cluster. The field samples (replicates at each sampling site) were then grouped according to their clusters of affiliation and were addressed regarding each sediment property. The distribution of each group of samples was

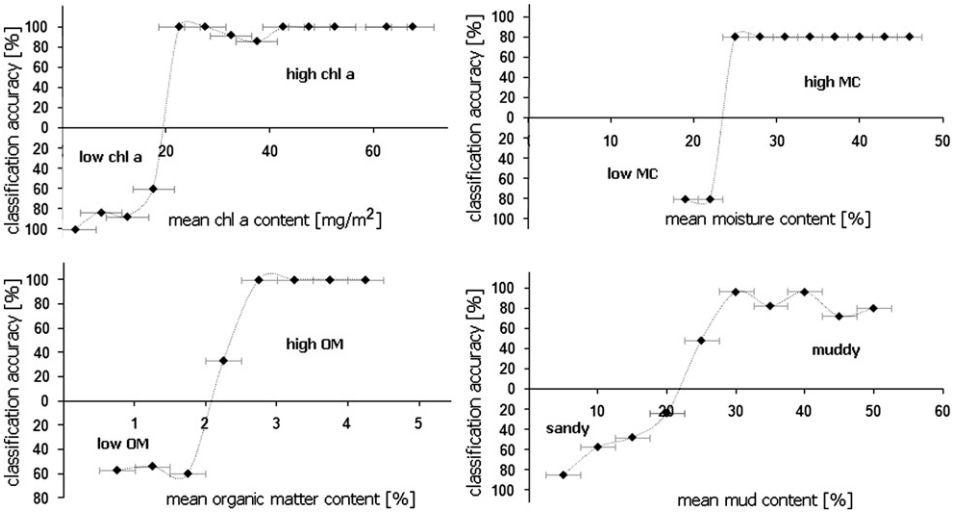

Fig. 5. The classification accuracy of field data with respect to ranges (5 mg/m^2 for chl *a* content, 3% for MC, 0.5% for OM, and 5% of MUC) of a property's content as derived from the Landsat TM and ETM+ settings.

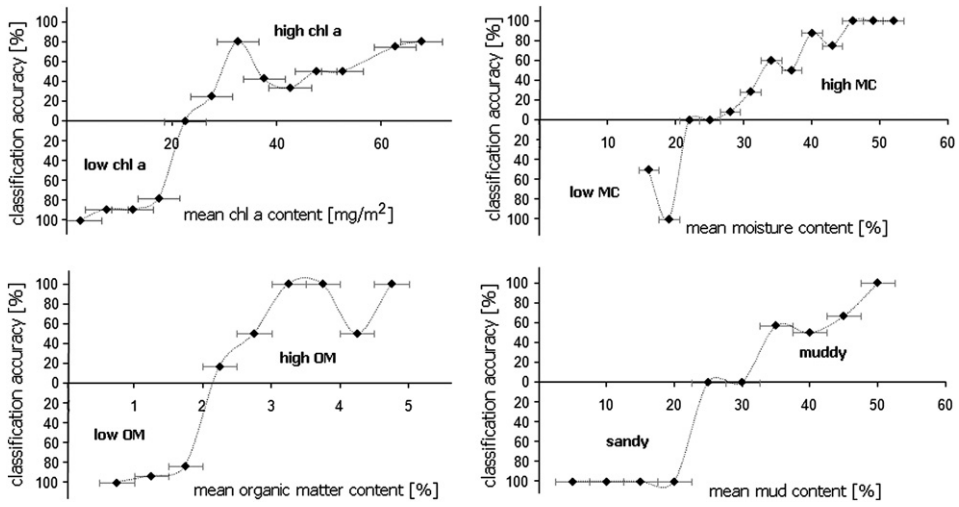

Fig. 6. The classification accuracy of field data with respect to ranges (5 mg/m^2 for chl *a* content, 3% for MC, 0.5% for OM, and 5% of MUC) of a property's content as derived from IKONOS settings.

checked per property. Based on these distributions, spectrally significant thresholds could be chosen per property, representing the spectral distinction of each group. All the field samples were then divided between these groups per property and were analyzed for their classification accuracy.

4. Results and discussion

4.1. Classification of the original image

The hyperspectral image resulted in 10 clusters using the NEC hierarchical approach with JM values ranging from 1.85 to 2.0. The decision to stop the hierarchical clustering and retrieve the final number of clusters depended on the amount of splitting needed to obtain various regions of interest of the Molenplaat.

Yet, since the concern of this analysis was to identify variations in mainly four sediment properties, it was essential to investigate how the sensors handled cluster separability with respect to those properties. The field data obtained from the Molenplaat covered only limited parts of the area, and therefore, they were included in a few clusters and in small numbers. In order to realize which properties were the most distinguishable, using each multispectral setting, the clusters with the lowest JM separability were merged until four clusters remained for the image. The decision to stop at four clusters was based on the need to have each cluster cover a "good" number of sampling sites while preserving the distinction between different spectral patterns on the Molenplaat.

Fig. 2 shows the four final clusters of the hyperspectral image. These clusters were of very high separability (JM $>$ 1.99). The field samples were found to be mainly distributed among three clusters labeled as: *a*, *b*, and *c*. The boundary cluster did not contain any field samples, yet, it showed very high separability with respect to the remaining clusters. Its presence does not affect the analysis but shows the most spectrally distinct clusters of the Molenplaat, and therefore, it is retained throughout the study.

Fig. 3 shows the distribution of field data within clusters using the mean property value for each cluster and the 10th and 90th percentile range of the data. Based on the distribution of the field data within the clusters, the following class-thresholds for each property were selected. Chl *a* content is "low" when lower than 20 mg/m^2 and "high" otherwise; moisture content is "low" when lower than 20% and *high* otherwise; organic matter content is "low" when lower than 2% and "high" otherwise; and finally a cluster was labeled as "sandy" sediment when mud content was lower than 20% and "muddy" sediment otherwise. It should be noted that the field samples that fell at the border of clusters were disregarded in the generation of Fig. 3, leading to 5 samples for cluster "*a*", 15 samples for cluster "*b*", and 24 samples for cluster "*c*".

Therefore, the three resulting clusters *a*, *b*, and *c* were respectively labeled as "low chl *a*, low MC, low OM, and sandy sediment", "low chl *a*, high MC, low OM, sandy sediment", and "high chl *a*, high MC, high OM, and muddy sediment".

In order to assess the accuracy of this classification with respect to the four sediment properties, the field data were divided into ranges of 5 mg/m^2 for chl *a* content, 3% for moisture content, 0.5% for organic matter content, and 5% of mud content. For each range, the percentage of correct classification of the included field samples was calculated. The results were a form of "*S*" curves, whereby a high classification accuracy would be found for the highest and lowest ranges of a sediment property. The values in between, and especially around the threshold used to form the two classes of a sediment property, were the more challenging areas to classify.

Fig. 4 shows the classification accuracy of the field data regarding each sediment property, within the specific ranges of the

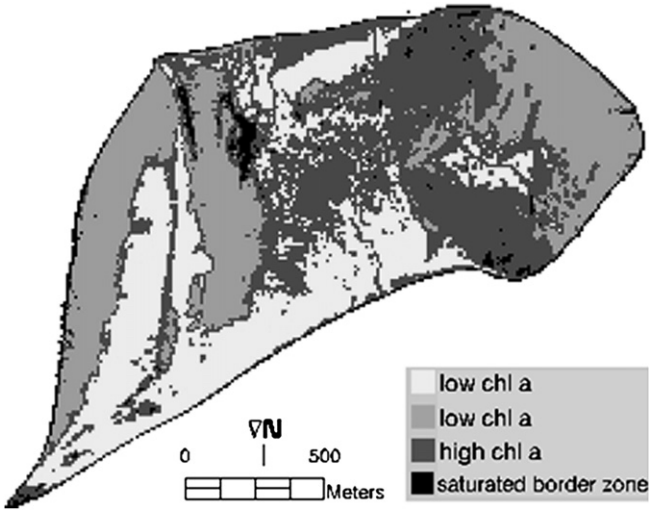

Fig. 7. The four final clusters of the MG classification of the hyperspectral image spatially resampled to Spot 5 HRG imagery, i.e. 10 m $\times$ 10 m.

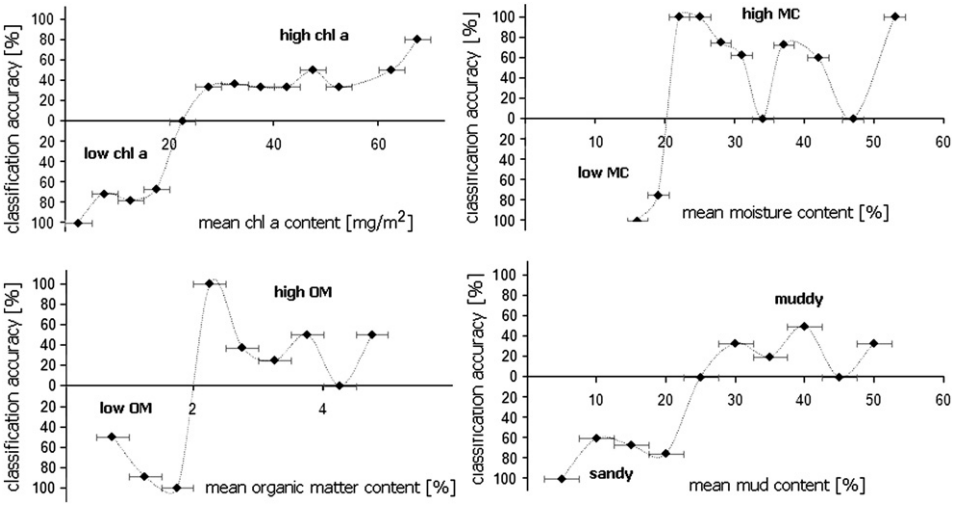

Fig. 8. The classification accuracy of field data with respect to ranges (5 mg/m^2 for chl *a* content, 3% for MC, 0.5% for OM, and 5% of MUC) of a property's content as derived from of the hyperspectral image spatially resampled to Spot 5 HRG imagery, i.e. 10 m × 10 m.

property's content. Regarding chl *a* and moisture content, the field data were mostly classified correctly, based on a 20% threshold between low and high contents of both properties. The lowest accuracy was for "low chl *a*" data as the content got closer to 20%. The field data in general were classified with lower accuracies when considering organic matter content and mud content.

4.2. Classification of the spectrally resampled images

The original image was resampled to the spectral properties of the four multispectral sensors. Then, these images were clustered by means of Mixture of Gaussians hierarchical approach. They resulted in several clusters that ranged between 8 and 12 clusters. The decision to stop the clustering depended on the amount of splitting needed to obtain various regions of interest of the Molenplaat. Although all the multispectral sensors were able to distinguish the major clusters of the hyperspectral image, the separability between these clusters differed between sensors: JM values ranging from 1.48 to 2.0 for Spot 5 HRG, 1.41 to 2.0 for Landsat 5 TM, 1.5 to 2.0 for Landsat 7 ETM+, and 1.1 to 2.0 for IKONOS.

Similarly to the approach used for the original hyperspectral image, the resulting clusters were merged into four. The four clusters for the Spot 5 HRG resampling had an acceptable separability (JM $>$ 1.78). Yet, the resulting patterns did not reveal information regarding the properties of interest. Based on the available knowledge of the area, it was not possible to label these resulting clusters, whereby further investigation is required to clarify their spectral significance. Aspects such as elevation and inclination of the Molenplaat and specific organic and inorganic matter in the sediment should be considered to investigate the distinction of these clusters by Spot 5 HRG. This cannot be addressed in the scope of this paper and this data set.

The spectral resampling to Landsat 5 TM and Landsat 7 ETM+ both resulted in four very similar clusters of high separability (JM $>$ 1.85). These clusters showed a distinction between variations in the considered properties with classification accuracy similar to that of the original image (Fig. 5).

When the IKONOS spectral bands were used, the four resulting clusters generally had a lower pairwise separability (JM $>$ 1.54). There was a decrease in classification accuracy of the properties compared to the original image (Fig. 6). There was a decrease in classification accuracy of chl *a* and organic matter content and a dramatic decrease regarding moisture content compared to using the hyperspectral data. This is due to IKONOS not covering a spectral band in the SWIR part of the spectrum, which is highly sensitive to moisture content. However, this classification was able to extract the saturated border zone which has an overall low spectral response.

4.3. Classification of the spatially resampled images

The original hyperspectral image was spatially resampled to the pixel size of the different sensors. Since the pixel size of IKONOS image is 4 m × 4 m, it is considered to have the same spatial resolution as the hyperspectral image. Fig. 7 and Fig. 9 show the resulting four clusters of the spatially resampled data using the hierarchical mixture of Gaussians scheme.

Unsupervised classification and its assessment were also used as a tool to evaluate the loss of spatial structures corresponding to different sediment properties when the hyperspectral image was resampled to the pixel size of Spot 5 HRG. The 10 m × 10 m hyperspectral image resulted in a good distinction between four different clusters (JM $>$ 1.990). On the other hand, there was no clear distinction between field data with respect to all sediment properties except for chl a (Fig. 8). This shows that a higher loss of

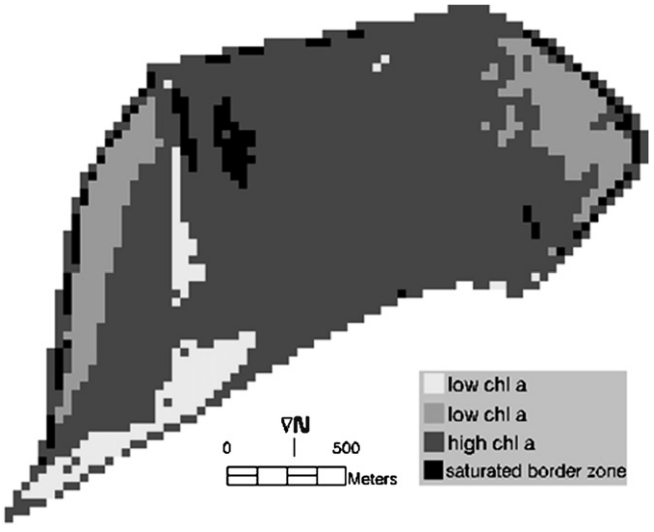

Fig. 9. The four final clusters of the MG classification of the hyperspectral image spatially resampled to Landsat imagery, i.e. 30 m × 30 m.

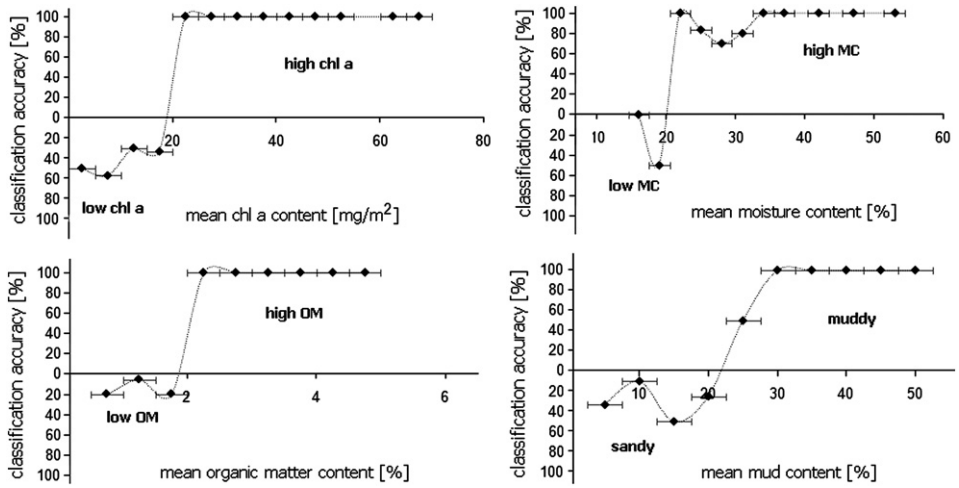

Fig. 10. The classification accuracy of field data with respect to ranges (5 mg/m^2 for chl *a* content, 3% for MC, 0.5% for OM, and 5% of MUC) of a property's content as derived from of the hyperspectral image spatially resampled to Landsat imagery, i.e. 30 m × 30 m.

Table 3
The performance of the multispectral data for sediment characterization on the Molenplaat compared to that of a hyperspectral image of 4 m × 4 m pixel size and 116 spectral bands: "+" indicates a comparable result and "−" indicates otherwise.

Sensor	Spectral applicability				Spatial applicability			
	MC	chl *a*	MUC	OM	MC	chl *a*	MUC	OM
Spot 5 HRG	−	−	−	−	−	+	−	−
Landsat5 TM	+	+	+	+	−	+	−	−
Landsat7 ETM+	+	+	+	+	−	+	−	−
IKONOS	−	−	+	+	+	+	+	+

spatial structure in the patterns of moisture content, organic matter content, and mud content occurred. Although the accuracy of chl *a* content decreased, the distinction between "high chl *a*" and "low chl *a*" areas was still possible. Therefore, compared to a 4 m × 4 m pixel size, the use of 10 m × 10 m mainly retains structures of chl *a* content.

Both Landsat settings are of the similar pixel size (30 m × 30 m). When resampled to the spatial settings of the Landsat sensors, the hyperspectral image resulted in a good distinction between four different clusters (JM > 1.999). On the other hand, a clear loss of detail is noticed, and most of the pixels in the image were grouped in one cluster. This is shown in Fig. 9 for both Landsat settings since they are of the same spatial resolution. Classification accuracy was much higher for high contents of each property due to the reason that most of the samples were extracted from areas of high moisture, organic matter, mud and chl *a* contents, and the cluster representing them is a dominant cluster. Therefore, it is more important to check the classification accuracy of the low content values of the different properties (Fig. 10). Using that approach, the only sediment property that seemed to be slightly retained was chl *a* content, whereby the clusters were only be labeled according to this sediment property (Fig. 9).

5. Conclusions

Sediment characterization by remote sensing should include efforts to utilize different sources of imagery for cost efficiency and temporal coverage. For this to occur in a reasonable manner, the choice of the different imagery has to be based on the their suitability for sediment characterization. In this paper, the suitability of multispectral sensors Spot 5 HRG, Landsat 5 TM, Landsat 7 ETM+, and IKONOS was assessed regarding sediment characterization of the Molenplaat. This investigation was carried out in comparison to a hyperspectral image consisting of 116 spectral bands and a 4 m × 4 m spatial resolution using unsupervised classification.

The hyperspectral image was spatially and spectrally resampled to the properties of the multispectral sensors. The field data covered only limited locations on the Molenplaat, whereby the properties of interest were moisture content, chlorophyll *a* content, organic matter content, and mud content. The resampled imagery were classified in an unsupervised manner and assessed for the characterization of these sediment properties. Table 3 shows the results of the different sensors compared to those of the hyperspectral image.

Landsat 7 ETM+ spectral settings showed the best results when compared to the hyperspectral image with a high JM separability between pairwise clusters. Furthermore, these settings led to a high quality distinction between variations in the considered sediment properties. Landsat 5 TM resulted in a lower JM separability between the clusters than that of Landsat 7 ETM+. Yet, it also resulted in high quality distinction between variations in the considered sediment properties. IKONOS led to a somehow "noisy" effect on the data. The clusters obtained were not of a high separability and showed a lower capability in detecting variations in most sediment properties, especially for moisture content. Finally, Spot 5 HRG generally resulted in a reasonable clustering, with an acceptable separability, yet the four most separable clusters were not connected to the variation in the four sediment types of interest.

Regarding the spatial aspect, IKONOS can obtain the same attributes as the hyperspectral image since it is of the same spatial resolution. On the other hand, mainly chl *a* patterns surfaced using the pixel sizes of the remaining sensors.

It is essential to keep in mind that this study was carried out starting from a 4 m by 4 m pixel size. There can be very important variations occurring on more detailed scales, especially when it comes to patterns in chl *a* content that can vary in patches that range from cm to m in size. Such scales were not addressed in this study due to constraints in the image resolution.

The presence of more field data that are well spread on the area can allow the utilization of more clusters and reveal in a better way the weaknesses and strength of the considered sensors. Yet, the current results already give guidelines regarding the usefulness of these sensors for the desired task.

Finally, these results give an indication regarding four spaceborne multispectral sensors to be used for sediment characterization of the Molenplaat. Yet, it might be necessary to apply different methods to different data types, especially for sensors that were revealed not to be suitable for this characterization.

Acknowledgments

The research presented in this paper is funded by the Belgian Science Policy Office in the frame of the STEREO II programme project SR/00/109 - ALGASED (remote sensing for characterization of inter-tidal sediments and microphytobenthic algae).

Partial support of this research is by the FP7 project THESEUS (Innovative technologies for safer European coasts in a changing climate).

The field and flight campaigns were supported by the Belgian Science Policy in the framework of the STEREO programme project SR/00/043, 072.

References

Adam, S., 2009. Bio-physical charactarization of sediment stability indicators for mudflats using remote sensing, Ph.D. thesis. Katholieke Universiteit Leuven, Belgium.

Adam, S., Vitse, I., Johannsen, C., Monbaliu, J., 2006. Sediment type unsupervised classification of the Molenplaat, Westerschelde estuary, the Netherlands. EARSeL eProceedings 5, 146–160.

Atkinson, P., Curran, P., 1995. Defining an optimal size of support for remote sensing investigations. IEEE Transactions and Geoscience and Remote Sensing 33, 768–776.

Atkinson, P., Tate, N., 2000. Spatial scale problems and geostatistical solutions: a review. The Professional Geographer 52, 1467–9272.

Austen, I., Andersen, T., Edelvang, K., 1999. The influence of benthic diatoms and invertebrates on the erodibility of an intertidal mudflat, the Danish Wadden Sea. Estuarine, Coastal and Shelf Science 49, 99–111.

Banfield, J., Raftery, A., 1993. Model-based gaussian and non-gaussian clustering. Biometrics 49, 803–821.

Barillé, L., Robin, M., Harin, N., Bargain, A., Launeau, P., 2010. Increase in seagrass distribution at Bourgneuf bay (France) detected by spatial remote sensing. Aquatic Botany 92, 185–194.

Beaven, S., Stein, D., Hoff, L., 2000. Comparison of gaussian mixture and linear mixture models for classification of hyperspectral data. In: Proceedings of the IEEE Geoscience and Remote Sensing Society, Honolulu, Hawaii.

Belluco, B., Camuffo, M., Ferrari, S., Modenese, L., Silvestri, S., Marani, A., Marani, M., 2006. Mapping salt-marsh vegetation by multispectral and hyperspectral remote sensing. Remote Sensing of Environment 105, 54–67.

Biernacki, C., Celeux, G., Govaert, G., Longrognet, F., 2006. Model-based cluster and discriminant analysis with the MIXMOD software. Computational Statistics & Data Analysis 51, 587–600.

Bozdogan, H., 1993. Choosing the number of component clusters in the mixture-model using a new informational complexity criterion of the inverse-fisher information matrix. Studies in Classification, Data Analysis, and Knowledge Organization, 40–54.

Bozdogan, H., 1994a. Choosing the number of clusters, subset selection of variables, and outlier detection in the standard mixture-model cluster analysis. New Approaches in Classification and Data Analysis, 169–177.

Bozdogan, H., 1994b. Mixture-model cluster analysis using model selection criteria and a new informational measure of complexity. In: Bozdogan, H. (Ed.), Multivariate Statistical Modelling. Proceedings of the First US/Japan Conference on the Frontiers of Statistical Modeling: An Informational Approach, vol. 2. Kluwer Academic Publishers, Dordrecht, the Netherlands, pp. 69–113.

Brockmann, C., Stelzer, K., 2008. Optical remote sensing of intertidal flats. In: Remote Sensing of the European Seas. Springer, pp. 117–128.

Bryant, R., Tyler, A., Gilvear, D., McDonald, P., Teasdale, I., Brown, J., Ferrier, G., 1996. A preliminary investigation into the spectral characteristics of inter-tidal estuarine sediments. International Journal of Remote Sensing 17, 405–412.

Carrère, V., Spilmont, N., Davoult, D., 2004. Comparison of simple techniques for estimating chlorophyll *a* concentration in the intertidal zone using high spectral-resolution field-spectrometer data. Marine Ecology Progress Series 274, 31–40.

Celeux, G., Soromenho, G., 1996. An entropy criterion for assessing the number of clusters in a mixture model. Journal of Classification 13, 95–212.

Choi, J.K., Ryu, J.H., Lee, Y.K., Yoo, H.R., Woo, H.J., Kim, C.H., 2010. Quantitative estimation of intertidal sediment characteristics using remote sensing and gis. Estuarine, Coastal and Shelf Science 88, 125–134.

Crawley, M., 2007. The R Book. Wiley.

Curran, P., 2001. Remote sensing: using the spatial domain. Environmental and Ecological Statistics 8, 331–344.

Dalponte, M., Bruzzone, L., Vescovo, L., Gianelle, D., 2009. The role of spectral resolution and classifier complexity in the analysis of hyperspectral images of forest areas. Remote Sensing of Environment 113, 2345–2355.

Dempster, A., Laird, N., Rubin, D., 1977. Maximum likelihood from incomplete data via the em algorithm. Journal of the Royal Statistical Society 39, 1–38.

Deronde, B., Kempeneers, P., Forster, R., 2006. Imaging spectroscopy as a tool to study sediment characteristics on a tidal sandbank in the Westerschelde. Estuarine, Coastal and Shelf Science 69, 580–590.

Doerffer, R., Murphy, D., 1989. Factor analysis and classification of remotely sensed data for monitoring tidal flats. Helgoländer Meeresunters 43, 275–293.

Dong, Z., Yan, L., Caiyun, Z., Liwei, H., Hao, S., Xiaoxin, M., 2005. Mapping intertidal sediments from space: a case study in Xiamen, China. Environmental Informatics Archives 3, 411–417.

ENVI, 2009. ENVI Reference Guide.

Foody, G., Sargent, I., Atkinson, P., Williams, J., 2004. Thematic labelling from hyperspectral remotely sensed imagery: trade-offs in image properties. International Journal of Remote Sensing 25, 2337–2363.

Ford, R., Honeywill, C., 2002. Grazing on intertidal microphytobenthos by macrofauna: is pheophorbide a useful marker? Marine Ecology Progress Series 229, 33–42.

Fraley, C., Raftery, A., 1998. How many clusters? which clustering method? answers via model-based cluster analysis. The Computer Journal 41, 578–588.

Herman, P., Middelburg, J., Heip, C., 2001. Benthic community structure and sediment processes on an intertidal flat: results from the ecoflat project. Continental Shelf Research 21, 2055–2071.

Huang, H., Liu, Y., Wang, B., 2010. Effect of spatial and spectral resolution of images on interpreting intertidal estuarine sediment grain size distributions. In: Geoscience and Remote Sensing Symposium (IGARSS). IEEE International, Honolulu, HI, p. 1316.

Hughes, G., 1968. On the mean accuracy of statistical pattern recognizers. IEEE Transactions on Information Theory 14, 55–63.

Hunt, G., 1977. Spectral signatures of particulate minerals in the visible and near infrared. Geophysics 42, 501–513.

Ibrahim, E., Adam, S., van der Wal, D., De Wever, A., Sabbe, K., Forster, R., Monbaliu, J., 2009. Assessment of unsupervised classification techniques for intertidal sediments. EARSeL eProceedings 8 (2), 158–179.

Ibrahim, E., Monbaliu, J., 2009. A Description of the Hyperspectral Imagery of ALGASED. Technical Report. The ALGASED Project.

Klein, D., Moll, A., Menz, G., 2005. Land cover/land use classification in a semiarid environment in east Africa using multi-temporal alternating polarisation envisat asar data. In: Lacoste, H., Ouwehand, L., (Eds), Proceedings of the 2004 Envisat & ERS Symposium (ESA SP-572). 6–10 September 2004, Salzburg, Austria.

Kostov, P., McErlean, S., 2006. Using the mixtures-of-distributions technique for the classification of farms into representative farms. Agricultural Systems 88, 528–537.

Lillesand, T., Kiefer, R., 2000. Remote Sensing and Image Interpretation. John Wiley & Sons, Inc.

Mitchener, H., Torfs, H., 1996. Erosion of mud/sand mixtures. Coastal Engineering 29, 1–25.

Muller, E., Decamps, H., 2000. Modeling soil moisture-reflectance. Remote Sensing of Environment 76, 173–180.

Murphy, R., Tolhurst, T., Chapman, M., Underwood, A., 2005. Estimation of surface chlorophyll *a* on an emersed mudflat using field spectrometry: accuracy of ratios and derivative-based approaches. International Journal of Remote Sensing 26, 1835–1859.

Neema, D., Shah, A., Patel, A., 1987. A statistical model for light reflection and penetration through sand. International Journal of Remote Sensing 8, 1209–1217.

Rahman, A., Gamon, J., Sims, D., Schmidts, M., 2003. Optimum pixel size for hyperspectral studies of ecosystem function in southern California chaparral and grassland. Remote Sensing of Environment 84, 192–207.

Rainey, M., Tyler, A., Gilvear, D., Bryant, R., McDonald, P., 2003. Mapping intertidal estuarine sediment grain size distributions through airborne remote sensing. Remote Sensing of Environment 86, 480–490.

Ryu, J., Kim, C., Lee, Y., Won, J., Chun, S.S., Lee, S., 2008. Detecting the intertidal morphologic change using satellite data. Estuarine, Coastal and Shelf Science 78, 623–632.

Ryu, J., Na, Y., Won, J., Doerffer, R., 2004. A critical grain size for Landsat ETM+ investigations into intertidal sediments: a case study of the Gomso tidal flats, Korea. Estuarine, Coastal and Shelf Science 60, 491–502.

Sadowski, F., Sarno, J., 1976. Additional Studies of Forest Classification Accuracy as Influenced by Multispectral Scanner Spatial Resolution. Technical Report. ERIM 122700-4-R. Environmental Research Institute of Michigan, Ann Arbor, Michigan.

Schläpfer, D., Böerner, A., Schaepman, M., 1999. The potential of spectral resampling techniques for the simulation of apex imagery based on aviris data. In: Summaries of the Eighth Annual JPL Airborne Earth Science Workshop (CA).

Silva, J., Santos, R., Calleja, M., Duarte, C., 2005. Submerged versus air-exposed intertidal macrophyte productivity: from physiological to community-level assessments. Journal of Experimental Marine Biology and Ecology 317, 87–95.

Smith, G.M., Thomson, A.G., Möller, I., Kromkamp, J.C., 2004. Using hyperspectral imaging for the assessment of mudflat surface stability. Journal of Coastal Research 20, 1165–1175.

Sorensen, T., Bartholdy, J., Christiansen, C., Pedersen, J., 2006. Intertidal surface type mapping in the Danish Wadden sea. Marine Geology 235, 87–99.

Theodoridis, S., Koutroumbas, K., 1999. Pattern Recognition. Academic Press.

Thomson, A., Fuller, R., Sparks, T., Yates, M., Eastwood, J., 1998. Ground and airborne radiometry over intertidal surfaces: waveband selection for cover classification. International Journal of Remote Sensing 19 (6), 1189–1205.

Thomson, A., Fuller, R., Yates, M., Brown, S., Cox, R., Wadsworth, R., 2003. The use of airborne remote sensing for extensive mapping of intertidal sediments and saltmarshes in eastern England. International Journal of Remote Sensing 24, 2717–2737.

Weidong, L., Baret, F., Xingfa, G., Qingxi, T., Lanfen, Z., Bing, Z., 2002. Relating soil surface moisture to reflectance. Remote Sensing of Environment 81, 238–246.

Woodcock, C., Strahler, A., 1987. The factor of scale in remote sensing. Remote Sensing of Environment 21, 311–332.

Yates, M., Jones, A., McGrorty, S., Goss-Custard, J., 1993. The use of satellite imagery to determine the distribution of intertidal surface sediments of the Wash, England. Estuarine, Coastal and Shelf Science 36, 333–344.